Editors' Suggestion

Enhanced skyrmion metastability under applied strain in FeGe

M. T. Littlehales,[1,2,*] L. A. Turnbull,[1] M. N. Wilson,[1,3] M. T. Birch,[4] H. Popescu,[5] N. Jaouen,[5] J. A. T. Verezhak,[6] G. Balakrishnan,[6] and P. D. Hatton[1]

[1]*Department of Physics, Durham University, DH1 3LE, United Kingdom*
[2]*ISIS Neutron and Muon Source, Rutherford Appleton Laboratory, Didcot, OX11 0QX, United Kingdom*
[3]*Department of Physics and Physical Oceanography, Memorial University, A1B 3X7, Canada*
[4]*Max-Planck-Institut für Intelligente Systeme, Heisenbergestraße, 70569, Stuttgart, Germany*
[5]*Synchrotron SOLEIL, Saint Aubin, Boîte Postale 48, 91192, Gif-sur-Yvette, France*
[6]*Department of Physics, University of Warwick, Coventry, CV4 7AL, United Kingdom*

(Received 5 October 2022; revised 24 November 2022; accepted 29 November 2022; published 26 December 2022)

Mechanical straining of skyrmion hosting materials has previously demonstrated increased phase stability through the expansion of the skyrmion equilibrium pocket. Additionally, metastable skyrmions can be generated via rapid field cooling to form significant skyrmion populations at low temperatures. Using small-angle x-ray scattering and x-ray holographic imaging on a thermally strained 200-nm-thick FeGe lamella, we observe temperature-induced strain effects on the structure and metastability of the skyrmion lattice. We find that in this sample orientation ($H \parallel [\bar{1}\,1\,0]$) with no strain, metastable skyrmions produced by field cooling through the equilibrium skyrmion pocket vanish from the sample upon dropping below the well-known helical reorientation temperature. However, when strain is applied along the [1 1 0] axis, and this procedure is repeated, a substantial volume fraction of metastable skyrmions persist upon cooling below this temperature down to 100 K. Additionally, we observe a large number of skyrmions retained after a complete magnetic field polarity reversal, implying that the metastable energy barrier protecting skyrmions from decay is enhanced.

DOI: 10.1103/PhysRevB.106.214434

I. INTRODUCTION

Magnetic skyrmions, nanometric vortexlike whirls of magnetization, typically exist in chiral magnets [1,2] under specific temperature and magnetic field conditions [3–5]. Skyrmions are normally stabilized by the competition of direct exchange, the Zeeman interaction, thermal fluctuations, and the Dzyaloshinskii-Moriya interaction (DMI), which requires a noncentrosymmetric crystal structure as present in conventional helimagnetic systems, such as MnSi [3], FeGe [6], and the insulating ferrimagnet Cu_2OSeO_3 [7]. Characterized by an integer winding number, skyrmions arrange in a periodic hexagonal crystal in two dimensions with a tubelike nature in the third dimension [8,9]. Their structure, size, and dynamical properties indicate promise for skyrmions as elements in complex computing devices, such as skyrmion racetrack memory [10,11], logic gates [12], Boolean processors [13], skyrmion transistors [14], as well as neuromorphic [15], stochastic [16], and reservoir computing [17].

A number of methods have been demonstrated to increase the size of the skyrmion equilibrium pocket to lower temperatures and higher magnetic fields [18,19]. For example, reducing the thickness of the system along the applied field direction can expand the skyrmion equilibrium region by suppressing the conical phase [20,21]. Additionally, metastable skyrmion states with near-infinite lifetimes can be formed by rapid field cooling through the equilibrium region to low temperatures [4,22,23]. Although not the energy minimum of the system, metastable states with large energy barriers present a greater operating region in which skyrmions may be manipulated for potential future device applications.

As a near-room-temperature skyrmion host, FeGe is a promising candidate for the above-mentioned devices. However, a major consideration in engineering novel spintronic applications lies in exploiting extrinsic effects, such as mechanical strain [24]. As the magnetic spin configuration in any material is fundamentally dependent on the underlying crystal structure, understanding the connection between magnetism and mechanical strain, known as magnetoelastic coupling, is paramount. Recent studies investigating strain effects on skyrmion spin textures have demonstrated anisotropic modulations of the skyrmion lattice, effectively modulating the DMI and exchange strength [25,26]. Similar anisotropic DMI has been observed in antiskyrmion systems caused by the D_{2d} crystal symmetry [27,28]. As a consequence of these energetic changes, mechanical strain can increase the skyrmion stability region [29,30] (as also seen for applied uniaxial pressure [19]) with Monte Carlo simulations of anisotropic DMI supporting these results [31,32]. Additionally, there are reports of room-temperature skyrmions existing in strain-engineered FeGe thin films [33]. These results also point to a method of direct skyrmion creation, via voltage-controlled application of strain with piezoelectric substrates [34,35].

In this paper, we employ resonant x-ray holography [36,37] to image the real-space magnetization [38] of metastable

*Corresponding author: matthew.t.littlehales@durham.ac.uk

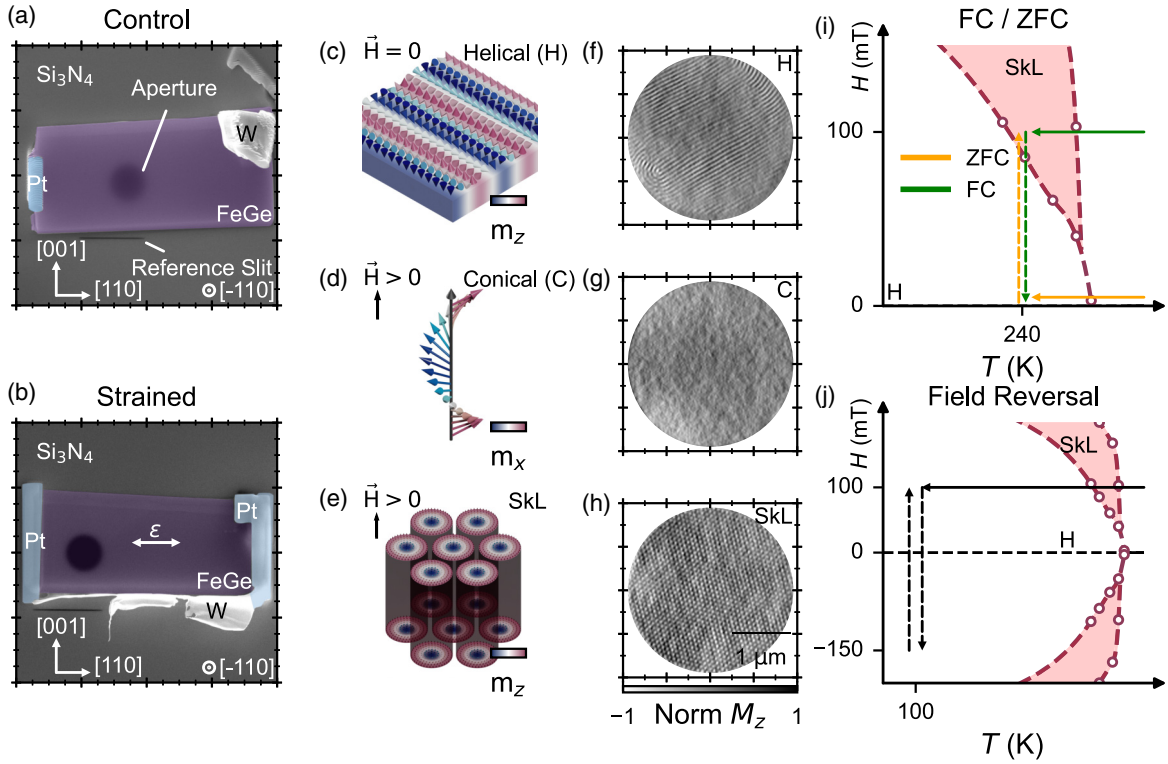

FIG. 1. (a) and (b) Scanning-electron-microscopy images of control and strained lamellae, respectively. Darker patches in the substrates represent a 3-μm diameter circular aperture and 6-μm long and 15-nm-wide reference slits milled through the substrates using focused ion-beam milling. Purple indicates the FeGe lamellae, blue indicates the platinum strips, and white indicates the tungsten remaining from the omniprobe micromanipulator detachment. (c)–(e) Schematics of spin textures present within the lamellae, (c) helical (H), (d) conical (C), and (e) skyrmion lattice (SkL). (f)–(h) X-ray holographic reconstructions of spin textures in FeGe lamellae corresponding to the illustrations in (c)–(e). (i) and (j) Phase diagram schematics of cooling protocols used within this paper. (i) Zero-field-cooled (ZFC) protocol including cooling in zero-field to 240 K then increasing magnetic field to 100 mT (orange) and field-cooled (FC) protocol at 100 mT to 240 K with a reduction in magnetic field to 0 mT (green). (j) Field-reversal protocol including a field cool at 100 mT to 100 K followed by a reversal of the magnetic field to −150 mT and back to 100 mT.

skyrmion states under the effects of thermally induced tensile strain on lamellae of single crystal FeGe [39,40]. Through differential thermal contraction between the sample and the substrate, we confirm elliptical skyrmion lattice deformation using small-angle x-ray scattering (SAXS) and demonstrate enhanced metastability of the skyrmion lattice against helical reorientations [41–43] and magnetic field reversals.

II. EXPERIMENTAL DETAILS

Single crystals of FeGe were grown via the chemical vapor transport method using 2 g of prepared FeGe powder and 2 mg/cm^3 of iodine transport agent with the source maintained at 450 °C and a 50 °C temperature gradient across the length of the furnace. After a period of 1 to 2 weeks, several single crystals with dimensions $1.5 \times 1.5 \times 1.5$ mm^3 were obtained at the furnace cold end. Two 200-nm-thick lamellae were milled from one of the single crystals with [0 0 1] and [1 1 0] directions in the plane of the sample and [$\bar{1}$ 1 0] out of the plane of the lamella, using gallium focused ion-beam (FIB) milling. The substrate consisted of a 5×5-mm, 300-μm silicon chip with 200-nm-thick Si_3N_4 x-ray transparent windows masked with 600-nm sputter-coated Au to avoid detector saturation and minimize the x-ray background, which was then mounted on a copper holder. The lamellae were fixed to the Si_3N_4 windows using platinum deposition at room temperature. A 3-μm-diameter aperture and a centrally offset 6-μm-long and 15-nm wide reference slit [37] was milled through the Au mask using FIB milling as shown in Figs. 1(a) and 1(b).

A control sample was made by fixing a single edge of a lamella to allow free expansion and contraction with temperature [Fig. 1(a)]. The sample under strain was produced by attaching opposite ends as shown in Fig. 1(b). The silicon chip contracts more than FeGe when cooling, therefore tensile strain up to a maximum of 0.25% is produced at 100 K along the [1 1 0] direction (see the Appendix for details of strain calculations).

X-ray holography was undertaken using the COMET end station on the SEXTANTS beam line at the SOLEIL synchrotron using resonant soft x-ray scattering with both left and right circularly polarized x rays at the Fe L_3 edge with an energy of 705.4 eV. This energy provided maximal magnetic contrast to absorption ratio for samples of this thickness, with the x-ray magnetic circular dichroism contrast isolated using a subtraction of the two circularly polarized x-ray scattering patterns. Interference patterns between the circular aperture and the extended reference slit were detected on a 2048 ×

2048, 13.5-μm^2 pixel charge coupled device (CCD). With a sample-to-detector distance of 138 mm, this gives an effective q resolution of 1×10^{-3} nm^{-1} at this energy corresponding to a real-space pixel size of 24.4 nm. To obtain SAXS-equivalent measurements, we used the same samples and a short exposure time. Without reconstructing the images, we observed high intensity skyrmion magnetic satellites and were able to track their position and orientation in reciprocal space.

The samples were cooled to a base temperature of 100 K via a liquid-helium cryostat. Magnetic fields up to a maximum of 150 mT were applied using a four-pillar permanent magnet array. Schematics of helical, conical, and skyrmion phases are shown in Figs. 1(c)–1(e) with corresponding x-ray holograms shown in Figs. 1(f)–1(h). At low magnetic fields, we observe helical states, consisting of continuous rotations of the magnetic spins around a propagation vector as shown in Fig. 1(c). Under finite magnetic fields applied along the incident x-ray beam direction, the helical propagation vector rotates to align along the magnetic field direction, while each spin gains a component along the field direction to form a conical state [Fig. 1(d)]. Since the component of magnetization along the beam direction is constant, no variation in the magnetic contrast is observed in Fig. 1(g). Under specific temperatures and magnetic fields, we observe magnetic skyrmions as a sixfold arrangement of light contrast circles surrounded by a dark background as shown in Fig. 1(h).

To discern possible differences in the strain effects on metastable and equilibrium skyrmions, we employed three distinct field-cooling and sweeping procedures. In the ZFC and FC regimes, the samples were cooled from above the Curie temperature ($T_C \approx 278$ K) [6] under applied fields of 0 and 100 mT, respectively, to a target temperature of 240 K. The ZFC/FC procedures were followed by increasing/decreasing magnetic field sweeps at 240 K, with holographic images collected at regular intervals. A third procedure involved FC to 100 K followed by a magnetic field reversal, denoted here as FR, where the field was decreased to zero, the orientation switched with respect to the beam direction, then increased. Each procedure is denoted in the phase diagrams in Figs. 1(i) and 1(j) with solid arrows indicating cooling procedures and dashed arrows showing magnetic field changes. Metastable skyrmions were only formed during FC protocols, as the field-cooling history passed through the equilibrium skyrmion region.

III. RESULTS AND DISCUSSION

To accurately measure strain effects on magnetic skyrmions and associated magnetic textures, we utilized complementary real and reciprocal space techniques, SAXS and x-ray holography, allowing us to quantify both skyrmion distortion and enhanced metastability.

We first investigate strain-induced skyrmion lattice distortion using SAXS. By field cooling at 100 mT through the skyrmion pocket, we formed metastable skyrmions at low temperatures while inducing increased lamella strain with decreasing temperature due to differential thermal contraction. Magnetic scattering, corresponding to the interaction between circularly polarized x rays and the m_z component of the sample magnetization, is shown in reciprocal space as a map of

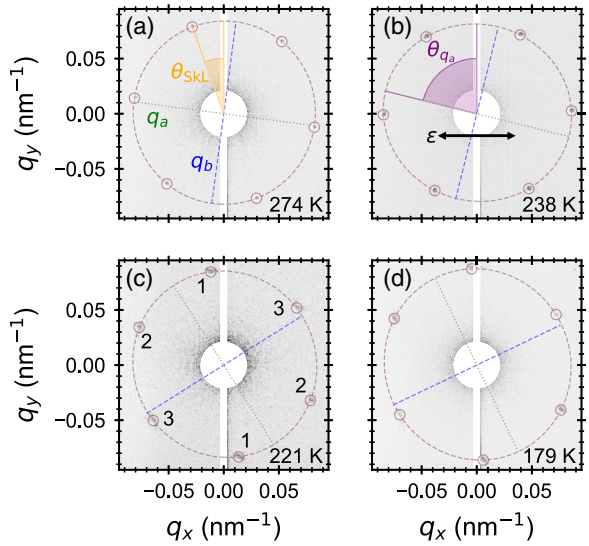

FIG. 2. (a)–(d) SAXS patterns of the strained FeGe lamellae at various temperatures. A white circle and a vertical rectangle are used to mask overspill of the main beam around the beam stop and scatter from the holography reference slit to aid in fitting procedures. The red dashed line shown in (a) represents an elliptical fit to the magnetic scattering peaks, the green dotted and blue dashed lines correspond to the semimajor (q_a) and semiminor axes (q_b), respectively. Skyrmion lattice orientation θ_{SkL} and ellipse orientation θ_{q_a} are measured anticlockwise from the vertical shown by orange lines in (a) and purple lines in (b). The strain direction in reciprocal space is represented by ε in (b). Pairs of skyrmion peaks are labeled in (c) corresponding to the analysis in Fig. 4(a).

the q_x, q_y plane. Consequently, characteristic sixfold skyrmion scattering patterns [3,23] are observed down to a base temperature of 100 K with a corresponding strain of 0.25% as seen in Figs. 2(a)–2(d).

With increasing strain, we observed elliptical distortion of the skyrmion lattice, alongside alignment of the skyrmion reciprocal space peaks along the strain direction [Fig. 2(b)], indicating strain dependence on both the structure and the orientation of the skyrmion lattice. By fitting an ellipse to the six magnetic satellites [44], we can characterize both the direction of the distortion in reciprocal space and its magnitude in the form of oblateness,

$$f = \frac{q_a - q_b}{q_a}, \tag{1}$$

where q_a and q_b correspond to the reciprocal length of the semimajor and semiminor axes of the ellipse, respectively [see Fig. 2(a), for example].

Within the equilibrium pocket, the estimated strain at 274 K [Fig. 2(a)] is 0.03% corresponding to an oblateness of $f = 0.01$: effectively an isotropic skyrmion lattice [Fig. 1(h)]. Figure 3(a) shows the resulting skyrmion oblateness as a function of increasing strain. We observe a linearly increasing distortion from room temperature to 230 K as shown in Fig. 3(a) at which point the distortion relaxes. Additionally, the reduction of q_b between 275 and 230 K [Fig. 3(b)] is indicative of the intrinsic helical winding length increasing along the [1 0 0] direction [see Fig. 2(b)], perpendicular to the strain. The divergence of q_a and q_b under increasing

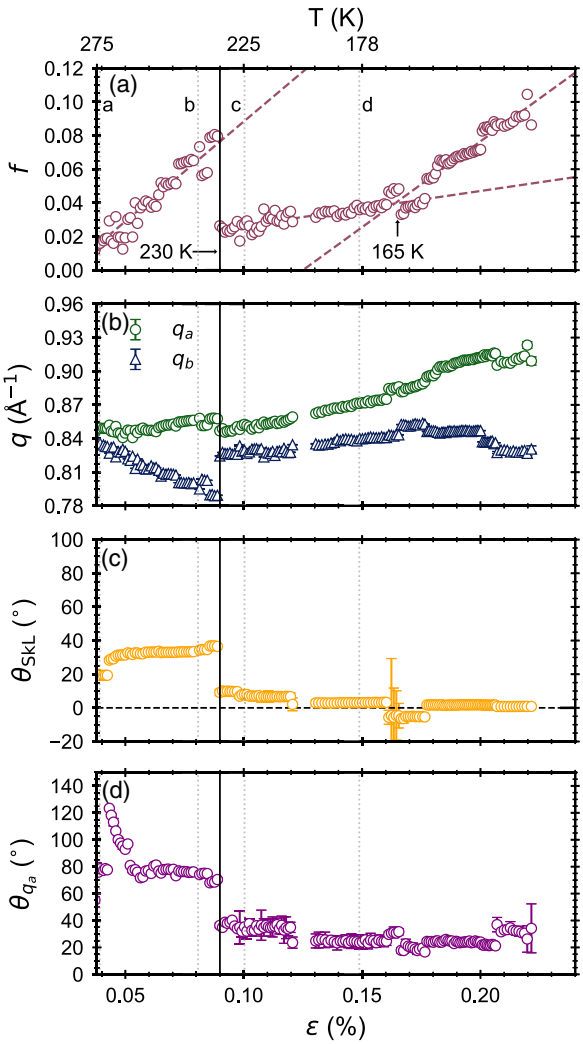

FIG. 3. Parameters measured during the 100 mT field cooling on the strained lamella. (a) Fitted ellipse oblateness as a function of increasing strain. Dashed lines indicate straight line fits to linear regions. (b) Semimajor (green circle) and semiminor (blue triangle) q-vectors q_a and q_b, respectively, of the fitted ellipses as a function of increasing strain. (c) Skyrmion lattice orientation θ_{SkL} versus strain. (d) Fitted ellipse orientation θ_{q_a} versus strain. Intrinsic reorientation of the magnetocrystalline anisotropy easy axes, indicated by black vertical lines at 230 K on each plot. Temperatures of SAXS patterns in Figs. 2(a)–2(d) are represented by labeled gray vertical dotted lines in panels (a)–(d) and labeled in panel (a).

tensile strain has previously been referred to as the skyrmion lattice "Poisson ratio" [26,45] and indicates that the magnetic state inherits the anisotropy of the crystal lattice distortion. Shibata *et al.*, have previously proposed the possibility of strain-induced anisotropic modulation to the DMI to account for this behavior [25], as the intrinsic helical winding length is described by $\lambda = 2\pi D/J$ where D is the DMI parameter and J is the exchange interaction strength. They argue that strain-induced modification to the exchange interaction is not sufficient to account for the magnitude of the anisotropy. Additionally, supporting first-principles calculations indicate that D is enhanced and hence q is suppressed [46], matching our observations.

At 230 K, the reduction in skyrmion lattice oblateness coincides with a distinct reorientation of the lattice [Fig. 3(c)], best represented by determining the angle from vertical, anticlockwise to the nearest magnetic peak as represented by the orange angle in Fig. 2(a). In FeGe, at approximately this temperature, the magnetocrystalline anisotropy easy axes reorient from the ⟨1 0 0⟩ directions to the ⟨1 1 1⟩ directions [41,42], in this case causing a reduction of the lattice distortion and a rotation of the skyrmion lattice. Increasing the strain shows a linear increase in lattice oblateness with a different gradient to the distortion from 275–230 K, as shown by the linear fits in Fig. 3(a), inferring that the energy term provided by strain is dependent on the crystallographic directions and, subsequently, the skyrmion orientation. This is supported by a further smaller reorientation at $\approx$ 165 K where the distortion gradient changes again, and we see a similar divergence of $q_{a,b}$ to the higher temperature effects [Fig. 3(b)], further evidence for a positive skyrmion Poisson ratio in FeGe. In addition, the orientation of the fitted ellipse as plotted in Fig. 3(d) shows a reorientation of the distortion direction from roughly the strain direction (allowing for some strain along the [0 0 1] direction), to approximately 54.7° from the strain axis. This is identical to the reorientation of the easy axes from [1 0 0] to [1 1 1], inferring that there is a dependence of the DMI anisotropy direction on the magnetocrystalline easy axes.

In Fig. 4(a), we plot the q vectors for each of the pairs of peaks as defined in Fig. 2(c). We observe an immediate oblateness in the ellipse at 275 K as shown in Fig. 2(a) due to a reduced q_1 vector with a component orthogonal to the strain direction. With increasing strain, both q_1 and q_2 remain approximately constant with q_3 linearly reducing until the easy axis reorientation at 230 K. After this reorientation, we observe all q vectors increase with reducing temperature, consistent with previous studies [23], with slightly different gradients. The strain dependence of q along the crystallographic axes shown in Fig. 4(a) shows that along the strain direction ($\parallel$ [1 1 0]), there is a linear increase in q, the gradient of which is similar both before and after the critical reorientation. In contrast, perpendicular to the strain direction ($\parallel$ [0 0 1]), we observe a steep decrease in q before the reorientation, corresponding to an enhancement in DMI in agreement with theoretical studies [46]. After the critical reorientation, $q \parallel$ [0 0 1] linearly increases with a steeper gradient than along the strain direction, inferring that DMI is diminished, providing further evidence for magnetocrystalline anisotropy directionality dependence on the strain-induced DMI anisotropy.

These results are further reflected in Fig. 4(c) where we observe a slight reduction in the total area of the ellipse with increasing strain followed by a large linear increase in the area after the easy-axis reorientation. This is indicative that there is a change in skyrmion size as a consequence of DMI anisotropy when there is a full volume fraction constrained through topological protection of the skyrmion number. After the reorientation, the system loses this constraint as a number of skyrmions are destroyed, allowing a reorientation of the skyrmions along a preferred direction, and arrange at their intrinsic spacing, dependent on (anisotropic) D and J.

Within this experimental geometry we were unable to decouple strain and temperature effects. The coupling between

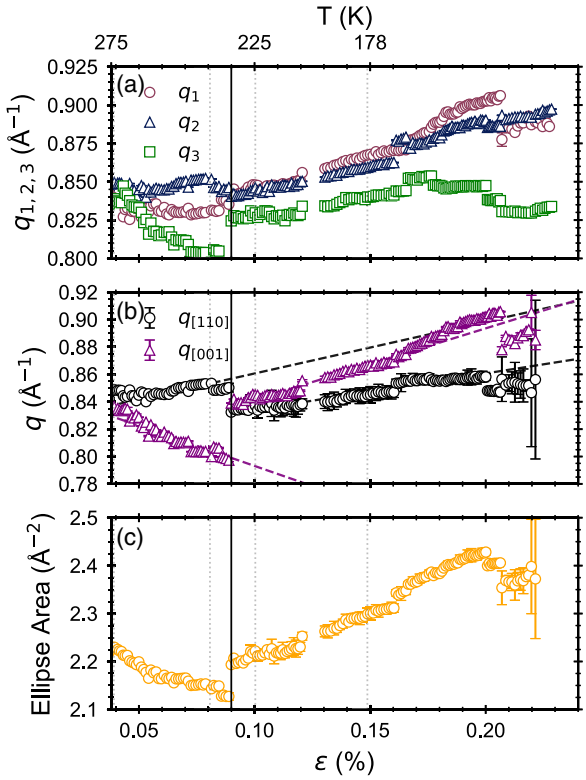

FIG. 4. (a) q_{1-3} vectors defined in Fig. 2(c) plotted as a function of increasing strain. (b) q vectors parallel to [1 1 0] (black circles) and [0 0 1] (purple triangles) versus strain. (c) Ellipse area calculated using area $= \pi q_a q_b$ versus strain. Intrinsic reorientation of the magnetocrystalline anisotropy easy axes indicated by black vertical line at 230 K on each plot. Temperatures of SAXS patterns in Figs. 2(a)–2(d) are represented by labeled gray vertical dotted lines in panels (a)–(d) and labeled in panel (a).

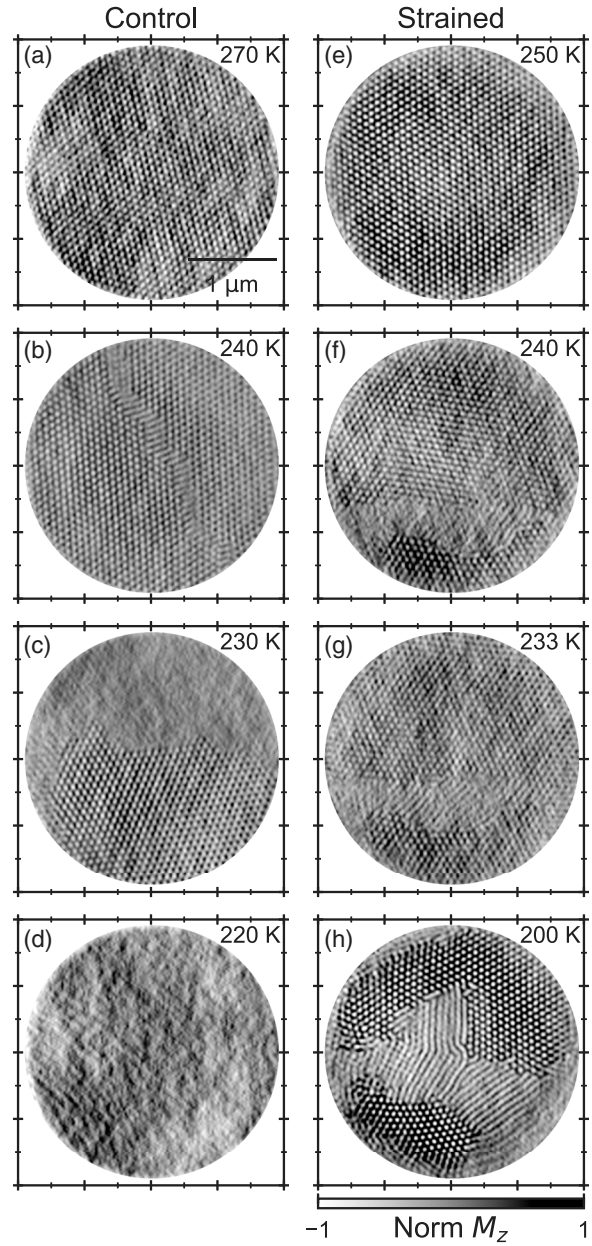

FIG. 5. (a)–(d) X-ray holographic images of skyrmion states in an unstrained lamella formed through a field-cooling process at 100 mT from 270 to 220 K. (e)–(h) Corresponding holographic images of a strained lamella through field cooling at 100 mT from 270 to 200 K.

temperature and strain causes a maximum oblateness of 0.1, found at 100 K, 0.25% strain, with a number of reductions in the maximum oblateness caused by temperature-induced reorientation. Within the freely expanding control sample, we observed a minimal amount of skyrmion lattice distortion up to an oblateness of 0.04 at 230 K (see the Supplemental Material [47]). This is attributed to a nominal amount of constriction formed by attaching one side of the lamella to the substrate. However, the large difference in the skyrmion distortion indicates that these results can be attributed to the straining of the lamella. In addition, we observed significant differences in the evolution and stability of the skyrmion lattice with respect to the helical reorientations and captured this using x-ray holography.

We performed holographic imaging of both samples when following a similar 100-mT field-cooling procedure from above T_C to 200 K. The images reveal the different evolutions of the volume fraction of skyrmions in the control and strained samples as exhibited in Figs. 5(a)–5(h). Interestingly, in the control lamella at 220 K, the skyrmion lattice suffers a complete volume fraction loss as shown in Fig. 5(d), indicating that the intrinsic easy-axis realignment provides enough energy to overcome the metastable energy barrier, in turn acting to unwind the skyrmion lattice. In comparison, skyrmions are retained within the strained lamella, which only suffers small volume fraction reductions as shown in Figs. 5(e)–5(g), to such an extent that at 200 K the skyrmion lattice is still present, coexisting with a complex helical domain [Fig. 5(h)]. The intrinsic easy-axis reorientation is, therefore, expected to raise the energy of the skyrmion state, thus, forcing a transition to the competing conical phase. However, with the addition of strain, the metastable energy barrier is increased such that the easy-axis reorientation does not provide enough energy to overcome the skyrmion to cone transition, therefore the skyrmions remain metastable.

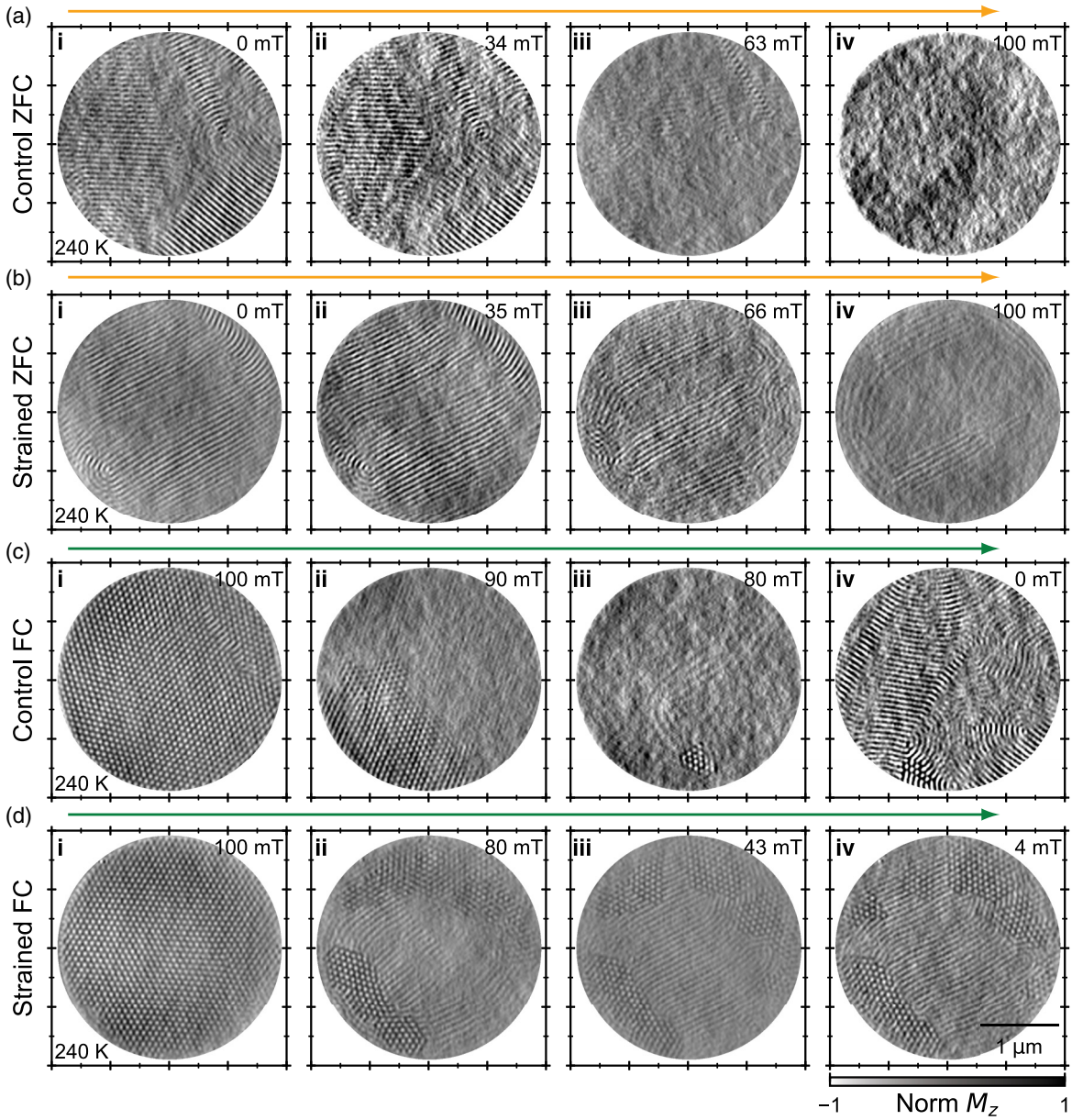

FIG. 6. (a) Holographic images of the ZFC protocol in the control sample measured at 240 K, (b) corresponding images taken in the strained sample after the identical procedure. (c) and (d) Images of FC sweeps in the control and the strained sample, respectively. Orange arrows indicate the increase in magnetic field after ZFC, green solid arrows indicate reduction in the magnetic field after FC.

Previous computational studies on strain in skyrmion systems suggests that the magnetoelastic coupling-induced anisotropic DMI acts to stabilize *A*-phase skyrmions to higher magnetic fields and lower temperatures [31,32]. To test this prediction, we performed ZFC and FC protocols as previously described and shown in Figs. 1(i) and 1(j). In the control ZFC at 240 K [Figs. 6(a,i)–6(a,iv)] with increasing magnetic field, we observe the ground-state helical phase at 0 mT [Fig. 6(a,i)] reduce in intensity until 100 mT where zero magnetic contrast corresponds to a conical phase with the wave vector aligned along the field direction, parallel to the incident beam direction. The corresponding ZFC sweep in the strained sample [Fig. 6(b,i)–6(b,iv)] indicates a similar phase evolution, however, at 100 mT, with a reduced volume fraction, the helical state still remains. This shows that both the previous field-cooled states in Fig. 5 were metastable and that the helical phase is stable up to higher out-of-plane magnetic fields.

Figure 6(c,i)–(c,iv) shows a magnetic field sweep from 100 to 0 mT after FC to 240 K to produce metastable skyrmions in the control sample. We observed significant volume fraction loss at 90 mT followed by only a small raft of skyrmions existing at 80 mT [Fig. 6(c,iii)]. Finally at 0 mT [Fig. 6(c,iv)], we observed a multidomain helical phase with six skyrmions present in the bottom of the aperture. Similar rafts of skyrmions have previously been observed by Tang *et al.* [48] through magnetic field reversals where up to 56 skyrmions were created within a bundle. Comparing to the strained case after FC, we observe over 200 skyrmions persisting after dropping the field to 0 mT with the most significant volume fraction loss observed in the initial field change to

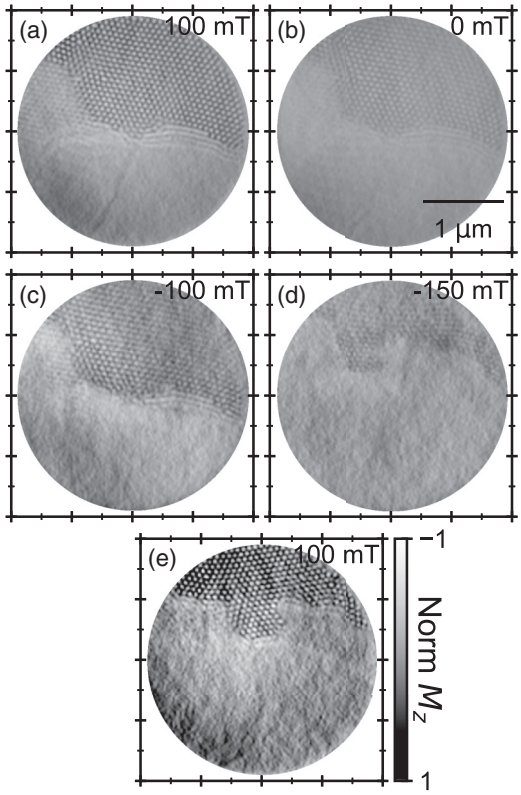

FIG. 7. (a)–(e) X-ray holographic images taken during FR protocol indicated in Fig. 1(j). Magnetic states are shown after a 100-mT field cool to 100 K, measured at (a) 100 mT , (b) 0 mT, reversing the direction of the magnetic field to (c) −100 mT, (d) −150 mT then back to the initial field at (e) 100 mT.

80 mT [Fig. 6(d,i)]. It can be seen that although large numbers of skyrmions are lost after the initial drop in the field, a greater number are retained to the lower magnetic fields within the strained sample. At this temperature, the calculated tensile strain of 0.06% causes an increase in the metastable energy barrier, thus enhancing the skyrmion metastability.

To investigate the extent of the enhanced metastability with increasing strain, we formed metastable skyrmions at 100 K by field cooling at 100 mT as indicated in Fig. 1(j), leading to a tensile strain of 0.25%. This formed an initial state shown in Fig. 7(a) with skyrmions present in the top half of the aperture, and a conical state in the bottom half, separated by a small boundary region of helical domains. Figures 7(a)–7(e) show a magnetic FR loop, dropping to negative fields, and returning back to positive fields, all while remaining at 100 K. Uncharacteristically, the skyrmions exist at all fields and are retained even after the magnetic field reversal. This is reminiscent of the skyrmion bundles observed by Tang *et al.*, [48] found after a magnetic FR in an unstrained 150-nm-thick FeGe lamella [48]. Our results show that much larger numbers of skyrmions are retained as a consequence of unaxial strain, potentially indicating that mechanical strain can be used to stabilize larger skyrmion bundles or other higher-order topological objects. Similar effects were not present within the control sample as the skyrmions decayed immediately as the field was reduced (see S.I [47]). Similarly, ZFC to 100 K and sweeping the magnetic field up to 100 mT in the control sample showed no signs of skyrmions, indicating that the effects observed can be attributed to strain effects on metastable magnetic phases.

IV. CONCLUSIONS

In conclusion, we have investigated mechanical strain effects on equilibrium and metastable skyrmions in FeGe lamellae using SAXS and x-ray holography. The evolution of a metastable skyrmion lattices as a function of decreasing temperature and increasing applied strain was tracked in order to observe effects on the structure and stability. We confirm that applied strain elliptically distorts the metastable skyrmion lattice and increases the metastability, allowing the field-cooled metastable lattice to withstand the well-known magnetic easy-axis switching from the ⟨1 0 0⟩ to the ⟨1 1 1⟩ directions. In contrast, nonstrained metastable skyrmions are destroyed in the easy-axis switching process, inferring that strain acts to increase the metastable energy barrier. Furthermore, the application of tensile strain at 100 K causes the metastable skyrmion lattice to survive against a magnetic field polarity flip with skyrmions surviving to high magnetic fields parallel to their core. Similarly, helices under tensile strain are maintained to higher magnetic fields, thus, enhancing the helical to conical energy barrier, potentially providing a method of improving the stability of skyrmions, skyrmion bundles, and other higher-order topological states.

ACKNOWLEDGMENTS

We acknowledge SOLEIL for provision of synchrotron radiation facilities and would like to thank H. Popescu and N. Jaouen for assistance in using beamline SEXTANTS. This work was supported by the UK Skyrmion Project EPSRC Programme Grant No. (EP/N032128/1). M.T.L. acknowledges the financial support of the Science and Technology Facilities Council (STFC) and the ISIS Neutron and Muon Source in the form of an ISIS facility development studentship.

APPENDIX: STRAIN ESTIMATION

The expected strain as a function of temperature is estimated using a simple model based on the differences in the thermal expansion coefficients of FeGe [49] and Si [50] plotted in Fig. 8(a). Assuming that the strain is uniaxial in the direction perpendicular to the constrained edges as shown in Fig. 1(b), the length with respect to temperature is given by the linear thermal expansivity,

$$\alpha_L = \frac{1}{L_0}\frac{dL}{dT} \quad \Rightarrow \quad L(T) = L_0 \int_{T_i}^{T_f} \alpha_L(T) dT, \qquad \text{(A1)}$$

where L_0 corresponds to the original length of the sample, $\alpha_L(T)$ corresponds to the temperature-dependent thermal expansivity, and $T_{i,f}$ corresponds to the initial and final temperatures, respectively. Assuming fixed boundary conditions at the sample edges enables strain calculation simplifications. This assumes that the substrate is unaffected by the thermal expansion in the FeGe lamella and that the final length of the lamella at any temperature is determined by the thermal

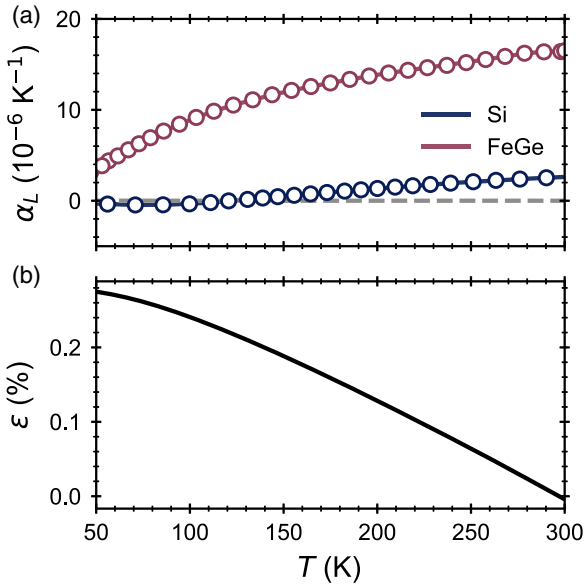

FIG. 8. (a) Thermal expansivities of Si (black) and FeGe (red) versus temperature [49,50]. (b) Estimated strain calulated using Eq. (A3).

contraction of the substrate alone. Consequently, the estimated strain is as follows:

$$\varepsilon = \frac{\Delta L}{L} = \frac{L_{\text{Substrate}}(T) - L_{\text{FeGe}}(T)}{L_{\text{FeGe}}(T)} \tag{A2}$$

$$= \frac{\int_{T_i}^{T_f} \alpha_{\text{Substrate}}(T)dT}{\int_{T_i}^{T_f} \alpha_{\text{FeGe}}(T)dT} - 1. \tag{A3}$$

The Si_3N_4 substrate is mounted on a silicon plate much larger than the substrate itself. Therefore, the thermal expansion of the substrate here is dependent upon the thermal expansion of the underlying silicon plate. Subsequently, it can be assumed that the substrate terms in Eq. (A3) are relative to the silicon mounting plate rather than the Si_3N_4 membrane. The estimated strain as a function of temperature is plotted in black in Fig. 8(b). At 100 K a strain percentage of approximately 0.25% is expected as previously reported [25,30,51].

[1] N. Nagaosa and Y. Tokura, Topological properties and dynamics of magnetic skyrmions, Nat. Nanotechnol. **8**, 899 (2013).

[2] U. K. Rößler, A. N. Bogdanov, and C. Pfleiderer, Spontaneous skyrmion ground states in magnetic metals, Nature (London) **442**, 797 (2006).

[3] S. Mulbauer, B. Binz, F. Jonietz, C. Pfleiderer, A. Rosch, A. Neubauer, R. Georgii, and P. Böni, Skyrmion lattice in a chiral magnet, Science **323**, 915 (2009).

[4] H. Oike, A. Kikkawa, N. Kanazawa, Y. Taguchi, M. Kawasaki, Y. Tokura, and F. Kagawa, Interplay between topological and thermodynamic stability in a metastable magnetic skyrmion lattice, Nat. Phys. **12**, 62 (2016).

[5] P. Milde, D. Köhler, J. Seidel, L. M. Eng, A. Bauer, A. Chacon, J. Kindervater, S. Mühlbauer, C. Pfleiderer, S. Buhrandt, C. Schütte, and A. Rosch, Unwinding of a skyrmion lattice by magnetic monopoles, Science **340**, 1076 (2013).

[6] X. Z. Yu, N. Kanazawa, Y. Onose, K. Kimoto, W. Z. Zhang, S. Ishiwata, Y. Matsui, and Y. Tokura, Near room-temperature formation of a skyrmion crystal in thin-films of the helimagnet FeGe, Nature Mater. **10**, 106 (2011).

[7] S. Seki, X. Z. Yu, S. Ishiwata, and Y. Tokura, Observation of skyrmions in a multiferroic material, Science **336**, 198 (2012).

[8] M. T. Birch, D. Cortés-Ortuño, L. A. Turnbull, M. N. Wilson, F. Groß, N. Träger, A. Laurenson, N. Bukin, S. H. Moody, M. Weigand, G. Schütz, H. Popescu, R. Fan, P. Steadman, J. A. T. Verezhak, G. Balakrishnan, J. C. Loudon, A. C. Twitchett-Harrison, O. Hovorka, H. Fangohr *et al.*, Real-space imaging of confined magnetic skyrmion tubes, Nat. Commun. **11**, 1726 (2020).

[9] F. N. Rybakov, A. B. Borisov, and A. N. Bogdanov, Three-dimensional skyrmion states in thin films of cubic helimagnets, Phys. Rev. B **87**, 094424 (2013).

[10] A. Fert, V. Cros, and J. Sampaio, Skyrmions on the track, Nat. Nanotechnol. **8**, 152 (2013).

[11] R. Tomasello, E. Martinez, R. Zivieri, L. Torres, M. Carpentieri, and G. Finocchio, A strategy for the design of skyrmion racetrack memories, Sci. Rep. **4**, 6784 (2015).

[12] X. Zhang, M. Ezawa, and Y. Zhou, Magnetic skyrmion logic gates: conversion, duplication and merging of skyrmions, Sci. Rep. **5**, 9400 (2015).

[13] B. Paikaray, M. Kuchibhotla, A. Haldar, and C. Murapaka, Reconfigurable logic operations via gate controlled skyrmion motion in a nanomagnetic device, ACS Appl. Electron.Mater. **4**, 2290 (2022).

[14] S. H. Moody, M. T. Littlehales, J. S. White, D. Mayoh, G. Balakrishnan, D. A. Venero, and P. D. Hatton, Electric field controlled mechanism for the deflection of skyrmions, arXiv:2205.15961.

[15] K. M. Song, J.-S. Jeong, B. Pan, X. Zhang, J. Xia, S. Cha, T.-E. Park, K. Kim, S. Finizio, J. Raabe, J. Chang, Y. Zhou, W. Zhao, W. Kang, H. Ju, and S. Woo, Skyrmion-based artificial synapses for neuromorphic computing, Nat. Electron. **3**, 148 (2020).

[16] H. Zhang, D. Zhu, W. Kang, Y. Zhang, and W. Zhao, Stochastic Computing Implemented by Skyrmionic Logic Devices, Phys. Rev. Appl. **13**, 054049 (2020).

[17] D. Pinna, G. Bourianoff, and K. Everschor-Sitte, Reservoir Computing with Random Skyrmion Textures, Phys. Rev. Appl. **14**, 054020 (2020).

[18] A. Chacon, A. Bauer, T. Adams, F. Rucker, G. Brandl, R. Georgii, M. Garst, and C. Pfleiderer, Uniaxial Pressure Dependence of Magnetic Order in MnSi, Phys. Rev. Lett. **115**, 267202 (2015).

[19] Y. Nii, T. Nakajima, A. Kikkawa, Y. Yamasaki, K. Ohishi, J. Suzuki, Y. Taguchi, T. Arima, Y. Tokura, and Y. Iwasa, Uniaxial stress control of skyrmion phase, Nat. Commun. **6**, 8539 (2015).

[20] A. B. Butenko, A. A. Leonov, U. K. Rößler, and A. N. Bogdanov, Stabilization of skyrmion textures by uniaxial dis-

tortions in noncentrosymmetric cubic helimagnets, Phys. Rev. B **82**, 052403 (2010).

[21] S. X. Huang and C. L. Chien, Extended Skyrmion Phase in Epitaxial FeGe(111) Thin Films, Phys. Rev. Lett. **108**, 267201 (2012).

[22] M. N. Wilson, M. Crisanti, C. Barker, A. Štefančič, J. S. White, M. T. Birch, G. Balakrishnan, R. Cubitt, and P. D. Hatton, Measuring the formation energy barrier of skyrmions in zinc-substituted Cu_2OSeO_3, Phys. Rev. B **99**, 174421 (2019).

[23] M. N. Wilson, M. T. Birch, A. Štefančič, A. C. Twitchett-Harrison, G. Balakrishnan, T. J. Hicken, R. Fan, P. Steadman, and P. D. Hatton, Stability and metastability of skyrmions in thin lamellae of Cu_2OSeO_3, Phys. Rev. Res. **2**, 013096 (2020).

[24] N. Lei, T. Devolder, G. Agnus, P. Aubert, L. Daniel, J.-V. Kim, W. Zhao, T. Trypiniotis, R. P. Cowburn, C. Chappert, D. Ravelosona, and P. Lecoeur, Strain-controlled magnetic domain wall propagation in hybrid piezoelectric/ferromagnetic structures, Nat. Commun. **4**, 1378 (2013).

[25] K. Shibata, J. Iwasaki, N. Kanazawa, S. Aizawa, T. Tanigaki, M. Shirai, T. Nakajima, M. Kubota, M. Kawasaki, H. S. Park, D. Shindo, N. Nagaosa, and Y. Tokura, Large anisotropic deformation of skyrmions in strained crystal, Nat. Nanotechnol. **10**, 589 (2015).

[26] S. P. Kang, H. Y. Kwon, and C. Won, Elastic moduli and poisson's ratio of 2-dimensional magnetic skyrmion lattice, J. Appl. Phys. **121**, 203902 (2017).

[27] J. Jena, B. Göbel, T. Ma, V. Kumar, R. Saha, I. Mertig, C. Felser, and S. S. P. Parkin, Elliptical bloch skyrmion chiral twins in an antiskyrmion system, Nat. Commun. **11**, 1115 (2020).

[28] W. C. Li, Z. Q. Liu, J. Y. Chen, D. Xie, X. W. Yao, and Z. X. Deng, Anisotropy of exchange and Dzyaloshinskii-Moriya interactions effects on the stabilization of Néel-type skyrmions, Phys. Scr. **97**, 085818 (2022).

[29] A. S. Sukhanov, P. Vir, A. Heinemann, S. E. Nikitin, D. Kriegner, H. Borrmann, C. Shekhar, C. Felser, and D. S. Inosov, Giant enhancement of the skyrmion stability in a chemically strained helimagnet, Phys. Rev. B **100**, 180403(R) (2019).

[30] S. Seki, Y. Okamura, K. Shibata, R. Takagi, N. D. Khanh, F. Kagawa, T. Arima, and Y. Tokura, Stabilization of magnetic skyrmions by uniaxial tensile strain, Phys. Rev. B **96**, 220404(R) (2017).

[31] S. El Hog, F. Kato, H. Koibuchi, and H. T. Diep, Finsler geometry modeling and monte carlo study of skyrmion shape deformation by uniaxial stress, Phys. Rev. B **104**, 024402 (2021).

[32] S. El Hog, F. Kato, S. Hongo, H. Koibuchi, G. Diguet, T. Uchimoto, and H. T. Diep, The stability of 3d skyrmions under mechanical stress studied via monte carlo calculations, Results in Physics **38**, 105578 (2022).

[33] S. Budhathoki, A. Sapkota, K. M. Law, S. Ranjit, B. Nepal, B. D. Hoskins, A. S. Thind, A. Y. Borisevich, M. E. Jamer, T. J. Anderson, A. D. Koehler, K. D. Hobart, G. M. Stephen, D. Heiman, T. Mewes, R. Mishra, J. C. Gallagher, and A. J. Hauser, Room-temperature skyrmions in strain-engineered FeGe thin films, Phys. Rev. B **101**, 220405(R) (2020).

[34] J.-M. Hu, T. Yang, and L.-Q. Chen, Strain-mediated voltage-controlled switching of magnetic skyrmions in nanostructures, npj Comput. Mater. **4**, 62 (2018).

[35] H. Yan, Z. Feng, S. Shang, X. Wang, Z. Hu, J. Wang, Z. Zhu, H. Wang, Z. Chen, H. Hua, W. Lu, J. Wang, P. Qin, H. Guo, X. Zhou, Z. Leng, Z. Liu, C. Jiang, M. Coey, and Z. Liu, A piezoelectric, strain-controlled antiferromagnetic memory insensitive to magnetic fields, Nat. Nanotechnol. **14**, 131 (2019).

[36] S. Eisebitt, J. Lüning, W. F. Schlotter, M. Lörgen, O. Hellwig, W. Eberhardt, and J. Stöhr, Lensless imaging of magnetic nanostructures by x-ray spectro-holography, Nature (London) **432**, 885 (2004).

[37] M. Guizar-Sicairos and J. R. Fienup, Holography with extended reference by autocorrelation linear differential operation, Opt. Express **15**, 17592 (2007).

[38] G. van der Laan and A. I. Figueroa, X-ray magnetic circular dichroismâa versatile tool to study magnetism, Coord. Chem. Rev. **277-278**, 95 (2014).

[39] L. A. Turnbull, M. T. Birch, A. Laurenson, N. Bukin, E. O. Burgos-Parra, H. Popescu, M. N. Wilson, A. Štefančič, G. Balakrishnan, F. Y. Ogrin, and P. D. Hatton, Tilted x-ray holography of magnetic bubbles in MnNiGa lamellae, ACS Nano **15**, 387 (2021).

[40] L. A. Turnbull, M. T. Littlehales, M. N. Wilson, M. T. Birch, H. Popescu, N. Jaouen, J. A. T. Verezhak, G. Balakrishnan, and P. D. Hatton, X-ray holographic imaging of magnetic surface spirals in FeGe lamellae, Phys. Rev. B **106**, 064422 (2022).

[41] B. Lebech, J. Bernhard, and T. Freltoft, Magnetic structures of cubic FeGe studied by small-angle neutron scattering, J. Phys.: Condens. Matter **1**, 6105 (1989).

[42] V. Ukleev, O. Utesov, L. Yu, C. Luo, K. Chen, F. Radu, Y. Yamasaki, N. Kanazawa, Y. Tokura, T. H. Arima, and J. S. White, Signature of anisotropic exchange interaction revealed by vector-field control of the helical order in a FeGe thin plate, Phys. Rev. Res. **3**, 013094 (2021).

[43] S. H. Moody, P. Nielsen, M. N. Wilson, D. A. Venero, A. Štefančič, G. Balakrishnan, and P. D. Hatton, Experimental evidence of a change of exchange anisotropy sign with temperature in Zn-substituted Cu_2OSeO_3, Phys. Rev. Res. **3**, 043149 (2021).

[44] Z. L. Szpak, W. Chojnacki, and A. van den Hengel, Guaranteed ellipse fitting with a confidence region and an uncertainty measure for centre, axes, and orientation, J. Math. Imaging Vision **52**, 173 (2015).

[45] Y. Hu, X. Lan, and B. Wang, Nonlinear emergent elasticity and structural transitions of a skyrmion crystal under uniaxial distortion, Phys. Rev. B **99**, 214412 (2019).

[46] T. Koretsune, N. Nagaosa, and R. Arita, Control of dzyaloshinskii-moriya interaction in $Mn_{1-x}Fe_xGe$: A first-principles study, Sci. Rep. **5**, 13302 (2015).

[47] See Supplemental Material at http://link.aps.org/supplemental/10.1103/PhysRevB.106.214434 for details of the control sample and AC susceptibility measurements.

[48] J. Tang, Y. Wu, W. Wang, L. Kong, B. Lv, W. Wei, J. Zang, M. Tian, and H. Du, Magnetic skyrmion bundles and their current-driven dynamics, Nat. Nanotechnol. **16**, 1086 (2021).

[49] H. Wilhelm, A. O. Leonov, U. K. Rößler, P. Burger, F. Hardy, C. Meingast, M. E. Gruner, W. Schnelle, M. Schmidt, and M. Baenitz, Scaling study and thermodynamic properties of the cubic helimagnet FeGe, Phys. Rev. B **94**, 144424 (2016).

[50] K. G. Lyon, G. L. Salinger, C. A. Swenson, and G. K. White, Linear thermal expansion measurements on silicon from 6 to 340 K, J. Appl. Phys. **48**, 865 (1977).

[51] J. Wang, Y. Shi, and M. Kamlah, Uniaxial strain modulation of the skyrmion phase transition in ferromagnetic thin films, Phys. Rev. B **97**, 024429 (2018).